Earth and Planetary Science Letters 289 (2010) 220–231

Contents lists available at ScienceDirect

Earth and Planetary Science Letters

journal homepage: www.elsevier.com/locate/epsl

Long-period eccentricity control on sedimentary sequences in the continental Madrid Basin (middle Miocene, Spain)

Hemmo A. Abels [a,b,*], Hayfaa Abdul Aziz [a,b], Wout Krijgsman [b], Sander J.B. Smeets [a], Frederik J. Hilgen [a]

[a] Stratigraphy/Paleontology, Dept. of Earth Sciences, Utrecht University, Budapestlaan 4, 3584 CD, Utrecht, The Netherlands
[b] Paleomagnetic Laboratory 'Fort Hoofddijk', Dept. of Earth Sciences, Utrecht University, Budapestlaan 17, 3584 CD, Utrecht, The Netherlands

ARTICLE INFO

Article history:
Received 9 February 2009
Received in revised form 29 October 2009
Accepted 3 November 2009
Available online 22 November 2009

Editor: P. DeMenocal

Keywords:
astronomical forcing
continental paleoenvironments
cyclostratigraphy
eccentricity
middle Miocene
Madrid Basin
sedimentary sequence

ABSTRACT

The middle Miocene Valdearenas–Muduex section in the internally-drained, continental Madrid Basin (central Spain) is dated bio-magnetostratigraphically between 15.2 Ma and 11.5 Ma. The section contains two formation-scale, sedimentary sequences, that both consist of a siliciclastic lower part and a calcareous upper part. Siliciclastic sedimentation took place in distal floodplain and fluvial environments, while limestones resulted from carbonate precipitation in calcic soil profiles and in ephemeral lacustrine water bodies. Spectral analysis of the L* colour time series points to the influence of the ~405-kyr and 0.97-Myr eccentricity cycles, while the bases of the two calcareous intervals correlate to successive minima of the 2.4-Myr eccentricity cycle. The 405-kyr cycle lags maximum eccentricity, whereas the 0.97 and 2.4-Myr cycles lag minimum eccentricity, each by approximately a quarter of a cycle. No obliquity forcing is detected. The observed orbital configuration of 2.4-Myr minima at the base of limestone-dominated intervals is similar to a previously documented Late Miocene shift in the Teruel Basin of northeast Spain. Our results indicate that long-period eccentricity climate forcing may well be a significant player on long, tectonic time scales in continental basin fill.

1. Introduction

Orbital forcing of paleoenvironments is increasingly documented in well-dated, continental sediment records. The impact of precession, obliquity, and ~100-kyr and ~405-kyr eccentricity cycles is shown in lacustrine, palustrine, and floodplain successions around the Mediterranean Sea (Abdul Aziz et al., 2003, 2004; Abels et al., 2009a,b). Besides these relatively high-frequency orbital cycles, eccentricity and obliquity also include low frequency cycles, with periods of 0.97 Myr and 2.37 Myr for eccentricity and 172 kyr and 1.2 Myr for obliquity (Varadi et al., 2003; Laskar et al., 2004). These long-period cycles are more often linked to major Cenozoic climate events of Cenozoic age recorded in marine settings (Beaufort, 1994; Lourens and Hilgen, 1997; Shackleton et al., 1999; Wade and Pälike, 2004; Abels et al., 2005; Pälike et al., 2006; Holbourn et al., 2007). A similar impact in continental settings is thus likely. Long-period variability is shown in the lithological cyclicity of the Triassic continental Newark Basin, that was related to long-period eccentricity forcing (Olsen, 1986; Olsen and Kent, 1999). The lack of reliable astronomical target curves for the Triassic however hampered calibration of the Newark results to calculated eccentricity curves. The impact of long-period cycles has also been recognized in Neogene mammal assemblage records of Spain (Van Dam et al., 2006). Eccentricity minima of the 0.97-Myr and 2.37-Myr cycles are held responsible for cooler and more humid climate conditions, resulting in increased small-mammal turnover rates and supposedly in lake expansions. Renewed turnover acceleration took place during cooler and drier conditions at times of 1.2-Myr obliquity minima, suggesting that obliquity played a role in the termination of lake phases.

The Miocene infill in the largely endorheic continental Madrid Basin is characterised by formation-scale sequential units that are composed of a dominant siliciclastic lower and carbonate-rich upper part. These units are occasionally bounded by sedimentary disconformities. The cause of this sequential arrangement is enigmatic, although a tectonic origin has been suggested (Calvo et al., 1989a; Alonso Zarza et al., 1990, 1992a; Calvo et al., 1996). Poor age calibration hampers detailed comparison of these sequences with tectonic records or orbital target curves. Intra-basinal correlations depend on lithostratigraphic patterns substantiated by low-resolution biostratigraphic age constraints (Sesé et al., 1990; Montes et al., 2006). Here, we try to substantiate the role of long-period eccentricity and obliquity in this continental basin fill. Therefore, a composite section in the north-eastern segment of the basin containing two siliciclastic-carbonate sequences is studied. A detailed magnetostratigraphy is established to

* Corresponding author. Stratigraphy/Paleontology, Dept. of Earth Sciences, Utrecht University, Budapestlaan 4, 3584 CD, Utrecht, The Netherlands. Tel.: +31 302535125; fax: +31 302533486.
E-mail addresses: abels@geo.uu.nl (H.A. Abels), krijgsma@geo.uu.nl (W. Krijgsman), fhilgen@geo.uu.nl (F.J. Hilgen).

0012-821X/$ – see front matter © 2009 Elsevier B.V. All rights reserved.
doi:10.1016/j.epsl.2009.11.011

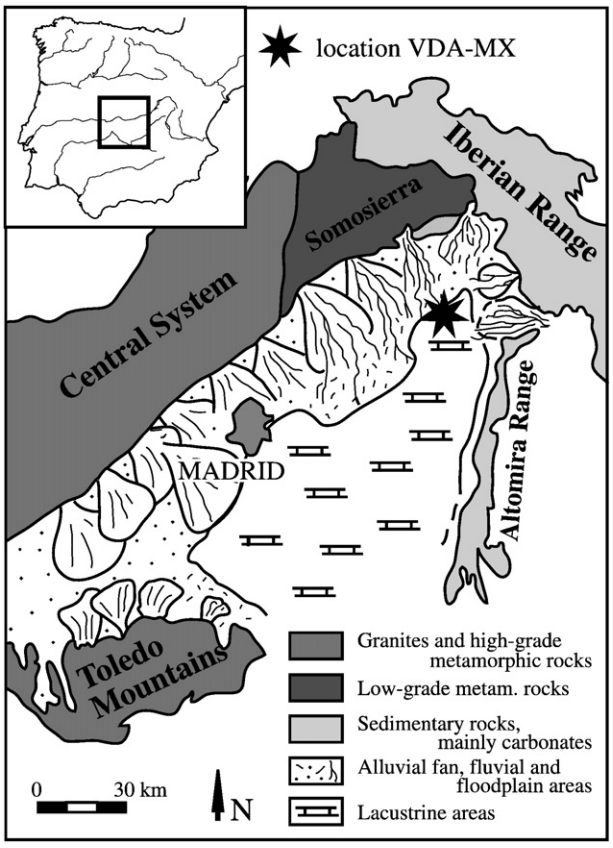

Fig. 1. Geological and paleoenvironmental map of the Madrid Basin during the deposition of the Intermediate Unit, modified after Alonso Zarza et al. (1992a,b). The location of the Valdearenas (VDA) and Muduex (MX) sections is indicated.

achieve accurate age control. High-resolution colour reflectance time series are generated and statistically analysed to detect orbital forcing of the sedimentary cycles. Finally, the sequential units are compared with orbital target curves and their intra- and inter-basinal significance was evaluated.

1.1. Geological setting

The ca 10,000 km^2 large Madrid Basin is located in central Spain, locked between the Central System in the northwest, the Iberian Range in the northeast, the Altomira Range in the east, and the Toledo Mountains in the south (Fig. 1; Calvo et al., 1989b). The basin originated from Alpine tectonics. The main tectonic phase started in the Late Oligocene as compressional and ended in the Late Miocene as extensional in ENE–WSW direction (Alonso Zarza, 1990). Miocene sediments unconformably overlie Paleogene and older rocks (Alonso Zarza et al., 1990). The total thickness of the Miocene sediments varies between 300 and 800 m from the margin to the centre of the basin. Small-mammal biostratigraphic control is poor, but indicates that sedimentation took place from 19 Ma to ~5 Ma (Alonso Zarza et al., 1990; Sesé et al., 1990; Pelaez-Campomanes et al., 2000). The Miocene basin infill is characterised by at least four to five sedimentary sequences that are found in three locally defined Units; one sequence in the Lower Unit, two or three sequences in the Intermediate (or Middle) Unit, and one in the Upper Unit (Calvo et al., 1989a,b; Alonso Zarza et al., 1990, 1992a; Cañaveras et al., 1996; Alonso Zarza and Calvo, 2002; Montes et al., 2006). Magnetostratigraphic data indicated a middle to Late Miocene age for the Lower and Intermediate Units in the central western and southern parts of the basin (Montes et al., 2006). In the north-eastern segment of the basin, the Intermediate Unit consists of two sequences both with a dominant siliciclastic lower part and carbonate-rich upper part. In the following, we refer to these two sequences as the lower and upper sequences.

1.2. Biostratigraphy

The biostratigraphic age constraints for the north-eastern segment of the basin available from scarce fossil mammal findings suggest a middle Miocene age for the Intermediate Unit. An overview of the most important mammal sites is given. The Pajares site is located east of our sections and is placed in the siliciclastic part of the lower sequence (Sesé et al., 1990). The site reveals small-mammal fauna that belongs to local zone D and lower MN5 (Sesé, 2006). The corresponding age is early middle Miocene, between 16 and 15 Ma according to the time scale of Daams et al. (1999). To the east of Guadalajara, near the village of Lupiana, the largest small-mammal association has been found in the siliciclastic part of the second sequence (Sesé et al., 1990). This association is characteristic of local sub-zone G3 that corresponds to a late middle Miocene age, between 12.8 and 11.1 Ma (Daams et al., 1999; Sesé, 2006). The Ledanca mammal site is closest to our section and located in the very top of the upper sequence, most probably just below the paleokarst surface (Sesé et al., 1990). The site yields fossil mammals related to local mammal zone H and lower MN9 that has an early Late Miocene age between 11.1 Ma and 10.4 Ma (Daams et al., 1999; Sesé, 2006).

2. Sections and lithology

The Valdearenas–Muduex composite section (VDA–MX) is composed of the Valdearenas section (VDA) that covers the lower sequence and the Muduex (MX) section that covers the lower and middle part of the upper sequence. Together they cover almost the entire Intermediate Unit. Poor outcrops of the upper sequence in the VDA section necessitated the 2.2 km NE lateral shift to the MX section. The correlation between the two sections cannot be done physically, and mainly depends on characteristics of limestone beds such as induration and stratigraphic pattern (Figs. 2 and 3). Both sections are located along the western flank of the Badiel river valley, close to the two villages after which the sections have been named. The sections have been part of earlier sedimentological studies (Alonso Zarza, 1990; Alonso Zarza et al., 1990; Sanz et al., 1995).

2.1. Valdearenas section

Siliciclastic sediments with limestone intercalations at meter scale dominate the basal 61 m of the 114 m thick VDA section (Figs. 2 and 3). Red and red-brown sandy mudstones display light-grey mottling and mm-size to cm-size carbonate nodules. Darker clay-rich and lighter sand-rich intervals occur. Few sandstone and gravel beds are present as sheet-like tabular beds, especially in the lower part of the siliciclastic interval, while some have a shallow channel-like geometry. Paleocurrent directions point to a S to SW transport direction (Alonso Zarza et al., 1990). Nodular and few prismatic, mottled, light-red calcareous beds intercalate at meter scale and occur at a fairly regular basis in the upper part of the siliciclastic interval (approximately every 3 to 5 m; limestone beds J to Q; Figs. 3C and 2).

The siliciclastic sediments have been interpreted as floodplain deposits of terminal fluvial systems (Alonso Zarza et al., 1990; Sanz et al., 1995), where sandstones relate to occasional enhanced fluvial activity and carbonate nodules are interpreted as of pedogenic origin. Intercalating calcareous levels have been interpreted to be related to carbonate precipitation in calcic paleosols that developed during times of low clastic input (Alonso Zarza et al., 1990; Sanz et al., 1995).

The siliciclastic interval is followed by a 43 m thick carbonate-rich interval of thick limestone beds with intercalations of marls and red mudstones (Fig. 2). This carbonate-rich interval represents the top part of the lower sequence (Fig. 2; Alonso Zarza et al., 1990). The

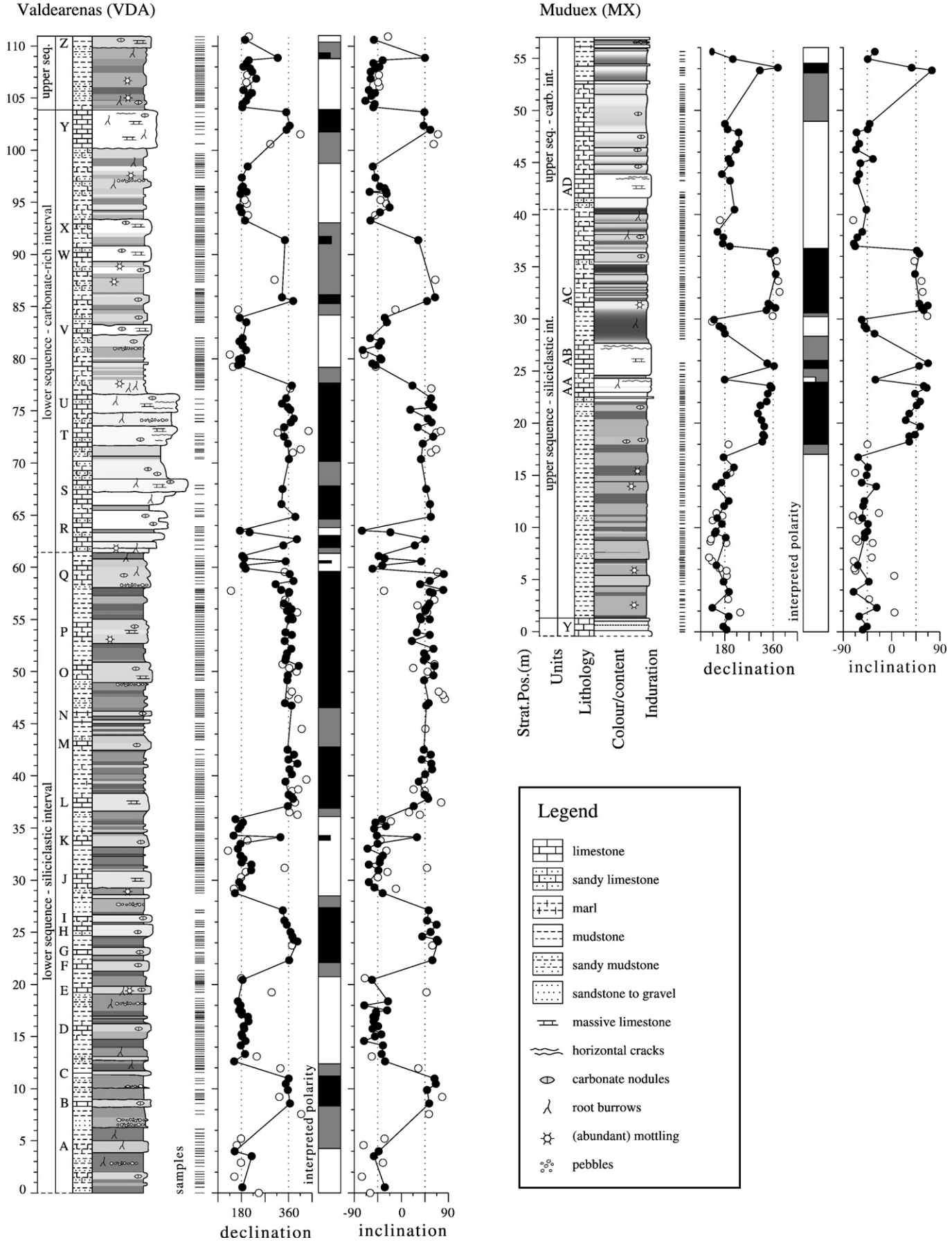
Valdearenas (VDA)
Muduex (MX)
upper seq.
lower sequence - carbonate-rich interval
lower sequence - siliciclastic interval
upper seq. - carb. int.
upper sequence - siliciclastic int.
AD
AC
AB
AA
Z
Y
X
W
V
U
T
S
R
Q
P
O
N
M
L
K
J
I
H
G
F
E
D
C
B
A
samples
interpreted polarity
declination
inclination
Strat.Pos.(m)
Units
Lithology
Colour/content
Induration
Legend
limestone
sandy limestone
marl
mudstone
sandy mudstone
sandstone to gravel
massive limestone
horizontal cracks
carbonate nodules
root burrows
(abundant) mottling
pebbles

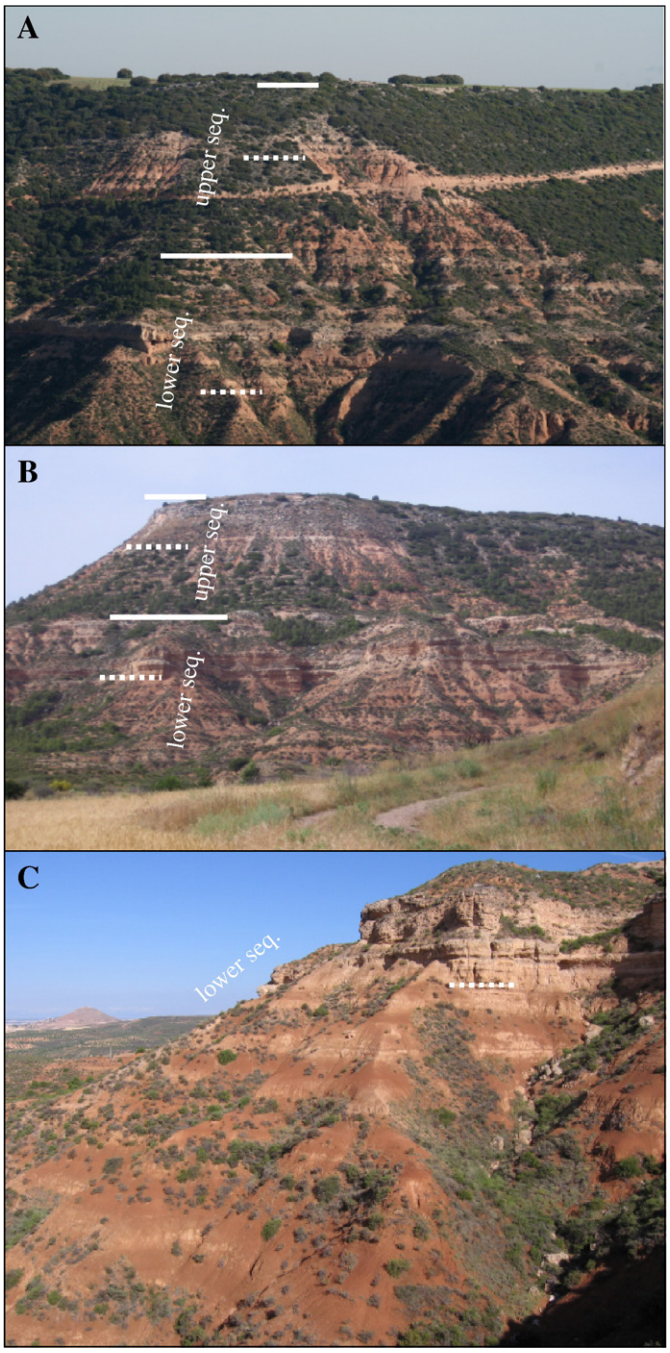

Fig. 3. (A–C) Photographs of the MX (A) and VDA sections (B and C). The transition from siliciclastic to carbonate-rich intervals in the lower and upper sequences is indicated with a dotted line.

limestone beds are up to 4 m thick, and display a change from nodular to prismatic and massive, mottled character. In the lower part of this interval, few limestone beds occur as tabular beds with a rather sharp, undulating base. The upper part of the carbonate-rich interval is characterised by smooth, extensively mottled limestones. The red to light-red mudstones that occur between limestone beds are rich in cm-scale carbonate nodules and display intense light-grey and yellow mottling. Both limestone and mudstone can be rich in sand- to gravel-sized material.

The high carbonate content of the intercalating mudstones has been interpreted as indication of continuous paleosol development during times of low clastic input (Sanz et al., 1995). The smooth, mottled limestones probably formed as typical palustrine limestones that relate to carbonate deposition in a pond environment that (subsequently) underwent sub-aerial exposure and pedogenic alteration (Alonso Zarza et al., 1990; Sanz et al., 1995).

2.2. Muduex section

The 57 m thick MX section covers 39 m of dominantly siliciclastic sediments followed by 18 m of carbonate-rich sediments. The siliciclastic interval in the MX section is sedimentologically fairly similar to the siliciclastic interval of the VDA section, however, it is less coarse, and has more dark clay-rich mudstones and carbonate beds. It is dominated by red to red-brown and brown mudstones that display light-grey and yellow mottling and dispersed carbonate nodules. Locally, levels rich in carbonate nodules occur and few smooth, mottled carbonate levels are intercalated. These levels are mostly smooth, massive limestone beds with a high carbonate content at the base that progressively decreases towards the top. These limestones are well-mottled and display rhizotubules and desiccation cracks (Alonso Zarza et al., 1990).

This siliciclastic interval is also interpreted as deposit of a distal floodplain environment with occasional paleosol and pond development (Alonso Zarza et al., 1990; Sanz et al., 1995). The higher clay and carbonate contents with respect to the siliciclastic part of the lower sequence are thought to indicate that more water is available in the system for paleosol or pond development during deposition.

The lower 13 m of the carbonate-rich interval is characterised by a dominance of limestone levels with occasional intercalation of brown, clayey mudstones. Locally, these intercalations occur at a smaller scale than in the lower sequence. Limestones are typically palustrine with extensive mottling and are interpreted as pond deposits (Alonso Zarza et al., 1990; Sanz et al., 1995). The upper 5 m of the carbonate-rich interval is characterised by red and green, clayey mudstones and very tabular, micritic limestone beds, in which gastropods and ostracods have been found (Alonso Zarza et al., 1990). These characteristics are prevalent for another approximately 20 m above the MX section, in which a progressive increase in number and thickness of the limestone beds is present. Silicified concretions occur in the very top of the studied part of the MX section. This upper interval, that has been referred to as the Carbonática Superior, is recognized over large parts in the north-eastern segment of the basin and is interpreted as widespread development of stable and (relatively) deep lacustrine conditions (Calvo et al., 1989a; Alonso Zarza et al., 1990). This interval was beyond the scope of our study.

3. Magnetostratigraphy

3.1. Methods

The composite VDA–MX section was sampled for magnetostratigraphy with an average sample spacing of 23 cm. Samples were drilled using an electric, water-cooled drill powered by a portable generator. First, every other sample was selected for demagnetization procedures. Later, sample resolution was increased for intervals that displayed polarity changes. The natural remanent magnetization (NRM) of the samples was measured on a horizontal 2G Enterprises DC SQUID cryogenic magnetometer (noise level 3×10^{-12} A/m) at the Paleomagnetic Laboratory "Fort Hoofddijk", Utrecht University, the Netherlands. The NRM was thermally demagnetized, using

Fig. 2. Lithological columns of the VDA and MX sections. The labelling of sequence intervals is indicated. To the right of the columns, the position of paleomagnetic samples, declination and inclination results of good quality (closed) and poor quality (open) interpreted ChRM are indicated as well as interpreted polarity, with normal (reversed) polarity in black (white) and uncertain polarity in grey.

incremental heating steps of 50° below and 30° above 240 °C, in a laboratory-built shielded furnace. Demagnetization results are plotted on orthogonal vector diagrams (Zijderveld, 1967) and characteristic remanent magnetization (ChRM) directions are calculated using principal component analysis (Kirschvink, 1980).

3.2. Results

Initial NRM intensities vary, depending on lithology, with high intensities (3 to 20 mA/m) in red mudstones and low to very low intensities (0.1 to 4 mA/m) in calcareous beds. The majority of the samples display good quality thermal demagnetization diagrams that allow to distinguish three components (Fig. 4). The first component is a randomly oriented, lab-induced, component that is removed below 120 °C. The second component is present in 99.4% of the samples and is removed between 200 °C and 270 °C (Fig. 4). This component has in all cases a normal polarity and is interpreted to represent a viscous overprint by the present day Earth's magnetic field. The third component displays dual polarities and is interpreted to represent the characteristic remanent magnetization (ChRM) of the sediment at times of deposition.

Approximately 18% of the samples have unblocking temperatures below 400 °C, suggesting iron sulphides as the main carrier of the ChRM (Fig. 4D). These samples mostly occur in the carbonate-rich intervals. The NRM of 43% of the samples is removed between 500 °C and 600 °C, which is the typical unblocking temperature range for magnetite (Fig. 4). Samples with this character are present in all types of sediments. The remaining 38% of the samples is fully demagnetized at temperatures from 600 °C up to 700 °C, indicating unblocking temperatures for (fine-grained) hematite. Samples with these unblocking temperatures are mostly derived from the red mudstones of the siliciclastic intervals. Only the samples that show a stable linear

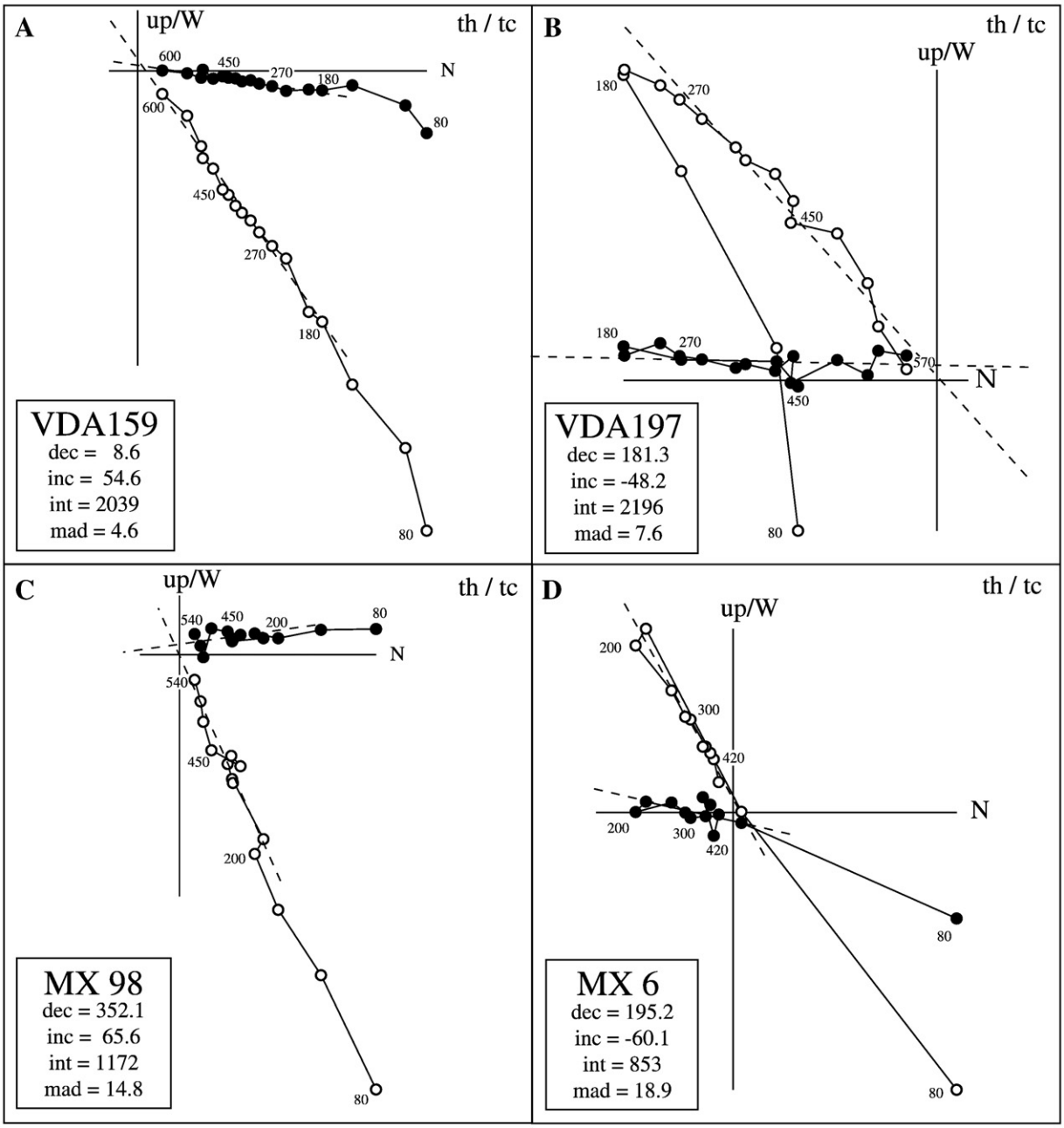

Fig. 4. (A–D) Zijderveld thermal demagnetization diagrams of two paleomagnetic samples of the VDA (A and B) and two of the MX section (C and D). Interpreted declination and inclination lines and values of the ChRM, and thermal steps are shown.

decay curve and clear normal or reversed-polarity components (solid dots in Fig. 2) have been used for the construction of the magnetic polarity pattern of the section.

3.3. Correlation to the ATNTS04

Declination and inclination data are plotted in stratigraphic order in Fig. 2. The magnetic polarity pattern of the composite section shows 9 normal-polarity intervals, labelled N1 to N9, and 10 reversed-polarity intervals, labelled R1 to R10. Polarity intervals defined by a single stratigraphic level (within R3, N4 and N7) are qualified as uncertain and are consequently not numbered. The middle part of the section is characterised by two successive long normal-polarity intervals (N3 and N4; Fig. 5). In accordance with the biostratigraphic age control (see Section 1.2), the most plausible correlation of N3 and N4 is to chrons C5ADn and C5ACn (ATNTS04; Fig. 5; Lourens et al., 2004). Consequently, the shorter N1 and N2 intervals correlate to chrons C5Bn.1n and C5Bn.2n, and intervals N7 and N8 to chrons C5An.2n and C5An.1n. The less well-resolved intervals N5 and N6 can be correlated to C5ABn and C5AAn. Apparently, the two short normal-polarity chrons C5Ar.1n and C5Ar.2n have not been resolved in our section (Fig. 2). Finally, we correlate the N9 polarity interval to C5r.2n.

Using the chron boundaries as age constraints allows the determination of sedimentation rates for the individual polarity intervals of the VDA–MX section (Fig. 5). Relatively constant sedimentation rates are present throughout the composite section, with lower rates in the carbonate-rich interval of the lower sequence. The upper sequence shows slightly lower rates than the lower sequence, while the transitional interval has remarkably low sedimentation rates. It must be noted, however, that the sedimentation rate in the MX section could be lower as the sections are located 2.2 km apart.

In summary, the magnetostratigraphic pattern in the VDA–MX section matches the polarity pattern in the geomagnetic polarity time scale rather well, allowing a straightforward correlation to the ATNTS04. This correlation is in good agreement with available biostratigraphic data (see Section 1.2) and resolves the sedimentation rate history of the area.

4. Cyclostratigraphy

4.1. Methods

The sedimentary cyclicity is studied using a high-resolution colour reflectance record as proxy for, mainly, carbonate content of the succession. The colour reflectance record was obtained by field-based measurements at 5-cm resolution using a portable photospectrometer (Minolta CM 508i). The measurements are based on the automatically calculated average of three measurements of the L* reflectance value and were taken in a straight line perpendicular to the bedding plane after removing the weathered material. L* reflects the lightness of the sediment and is therefore regarded to approximate the carbonate content.

Blackman–Tuckey (BT) spectral analysis was carried out using the Analyseries 1.1 program (Paillard et al., 1996). Significant frequency components in the BT spectrum were extracted from the time series using bandpass filters with the bandpass-width defined by lower and upper frequency limit of the target peak. BT Cross-spectral analysis was performed using 90% confidence limit, Barlett window, and compromise settings. The CLEAN algorithm was applied to the colour reflectance time series using the Mc-Clean program of Heslop and Dekkers (2002) with the red noise simulation type and standard settings. Reconstructed data series are automatically calculated by the Mc-Clean program above a chosen confidence level.

4.2. Colour records

The L* record mimics the lithological variations in the VDA–MX succession (Fig. 5) with higher values in the major carbonate levels. Specific patterns can be slightly different between the lithological log and the L* record, especially close to the boundaries of carbonate beds. Nevertheless, the L* record appears to be a good proxy for lithology in the VDA–MX section. Sedimentation rates are shown to vary slightly with sediment type (Fig. 5). Therefore, the colour depth records are converted into the time domain before proceeding with spectral analysis. Three age models were constructed using the magnetostratigraphic correlation to the ATNTS04 time scale, to explore the impact on the time domain if an increasing number of age calibration points are used whereby polarity reversals are added that are less accurately located in the section. Age model 1 employs a low, Age model 2 an intermediate, and Age model 3 a high number of age tie-points. Respective tie-points for the three age models are shown in Fig. 5 (see figure caption). Age model 1 has only three age tie-points and thus more or less reflects the original depth series as also evidenced by the results of spectral analysis in the depth domain, which are not shown here.

4.3. 405-kyr eccentricity forcing

The BT and CLEAN power spectra of the three colour time series are shown in Fig. 6. Spectral analysis results of the three L* time series reveal significant differences, indicating that the number of tie-points for age model construction is critical for the outcome of the analysis. Age models 2 and 3 show less noisy spectra than Age model 1, suggesting that a higher resolution time control results in a reduction of noise caused by changes in sedimentation rate.

In all spectra, significant peaks indicate cyclicity that might be related to the ca 405-kyr eccentricity cycle (Fig. 6). In Fig. 7, the extracted frequency components above the 99% confidence limits of the CLEAN spectra are shown next to the three L* time series and the eccentricity curve of Laskar et al. (2004). Also, the bandpass filters of the 405-kyr component of the L* time series are shown. Especially Age model 2 results in a fairly consistent phase relation with the 405-kyr eccentricity cycle. Cross-spectral analysis between the L* time series of Age model 2 and eccentricity shows a significant coherence with the 405-kyr eccentricity cycle (Fig. 8). The phase spectrum indicates that the L* record lags 405-kyr eccentricity by approximately a quarter of a cycle (Fig. 8). The ca 100-kyr eccentricity cycle does not reveal a significant coherence.

4.4. Low frequency cyclicity

A lower frequency component that corresponds to a period of approximately 0.8 to 1 Myr is also present in the spectra (Figs. 6 and 7). In the L* time series and the 99% reconstructed L* series of the CLEAN spectra, this component can be recognized by higher values of roughly every second 405-kyr cycle. This component might be related to the 0.97-Myr eccentricity and 1.2-Myr obliquity cycles. Comparison with the filtered components of both cycles reveals that this cycle is most likely related to the 0.97-Myr eccentricity cycle (Fig. 7). The lightest intervals and maxima in the filtered component of the L* time series reveal a lagged, opposite phase relation with the 0.97-Myr eccentricity cycle. The poor resolution in the low frequency realm, as a consequence of the limited length of the time series, does not permit comparison of the data with the 2.4-Myr eccentricity cycle in the frequency domain. Therefore, a filter of this eccentricity cycle is added to Fig. 5 for comparison with lithology. In the figure, the carbonate-rich intervals are indicated by grey-shaded areas that are correlated to the time domain. Clearly, the carbonate-rich parts of the lower and upper sequences both start during minima in eccentricity, at 14.2 Ma and 11.9 Ma, and continue for 1.2 Myr and at least 0.3 Myr,

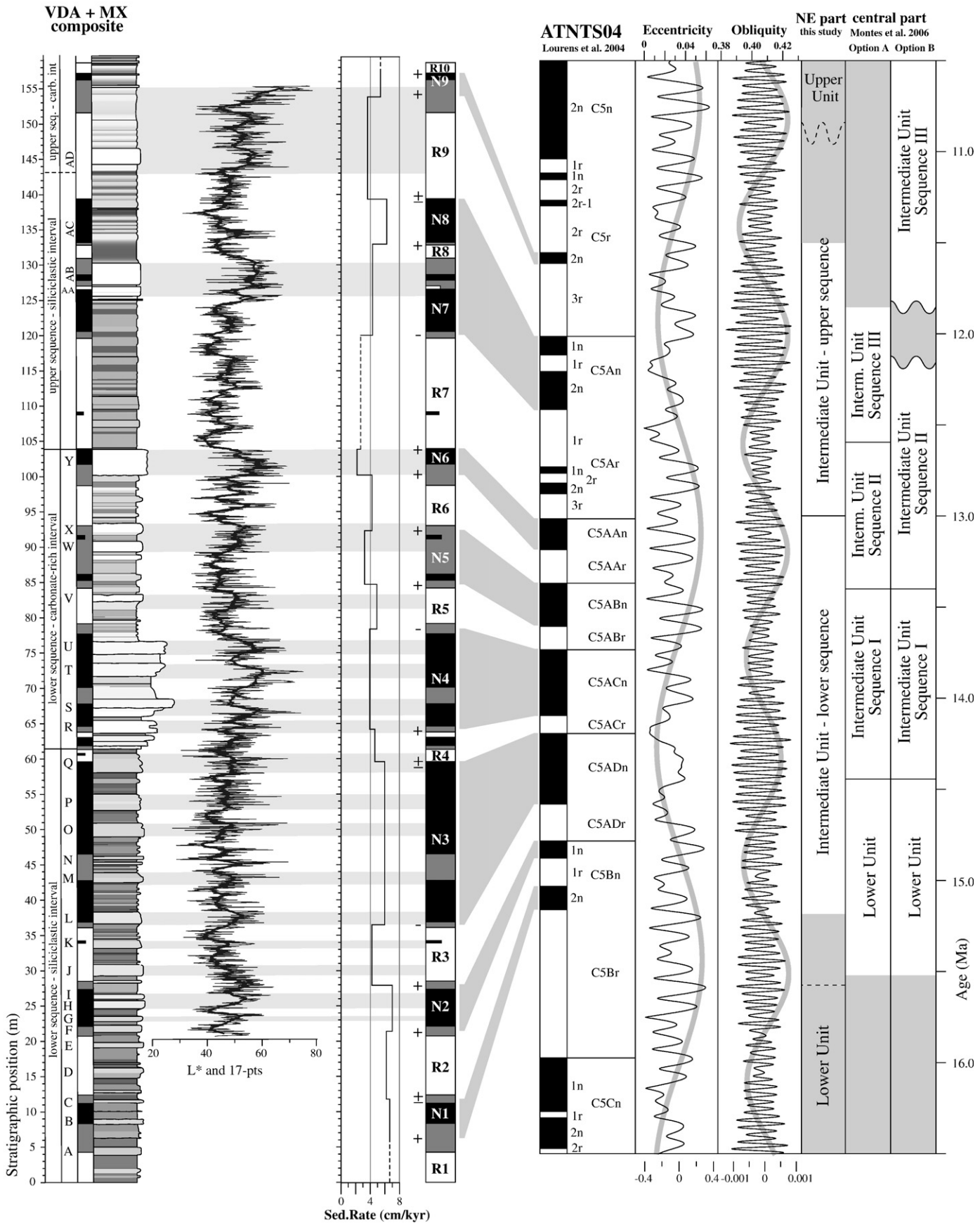
VDA + MX composite
Stratigraphic position (m)
upper seq. - carb. int
upper sequence - siliciclastic interval
lower sequence - carbonate-rich interval
lower sequence - siliciclastic interval
AD
AC
AB
AA
Y
X
W
V
U
T
S
R
Q
P
O
N
M
L
K
J
I
H
G
F
E
D
C
B
A
L* and 17-pts
Sed.Rate (cm/kyr)
R10
N9
R9
N8
R8
N7
R7
N6
R6
N5
R5
N4
R4
N3
R3
N2
R2
N1
R1
ATNTS04
Lourens et al. 2004
Eccentricity
Obliquity
NE part central part
this study
Montes et al. 2006
Option A Option B
2n C5n
1r
1n
2r
2r-1
2r C5r
2n
3r
1n
1r C5An
2n
1r
1n C5Ar
2r
2n
3r
C5AAn
C5AAr
C5ABn
C5ABr
C5ACn
C5ACr
C5ADn
C5ADr
1n
1r C5Bn
2n
C5Br
1n
C5Cn
1r
2n
2r
Upper Unit
Intermediate Unit - upper sequence
Intermediate Unit - lower sequence
Lower Unit
Lower Unit
Interm. Unit Sequence III
Interm. Unit Sequence II
Intermediate Unit Sequence I
Intermediate Unit Sequence I
Lower Unit
Intermediate Unit Sequence III
Intermediate Unit Sequence II
Age (Ma)

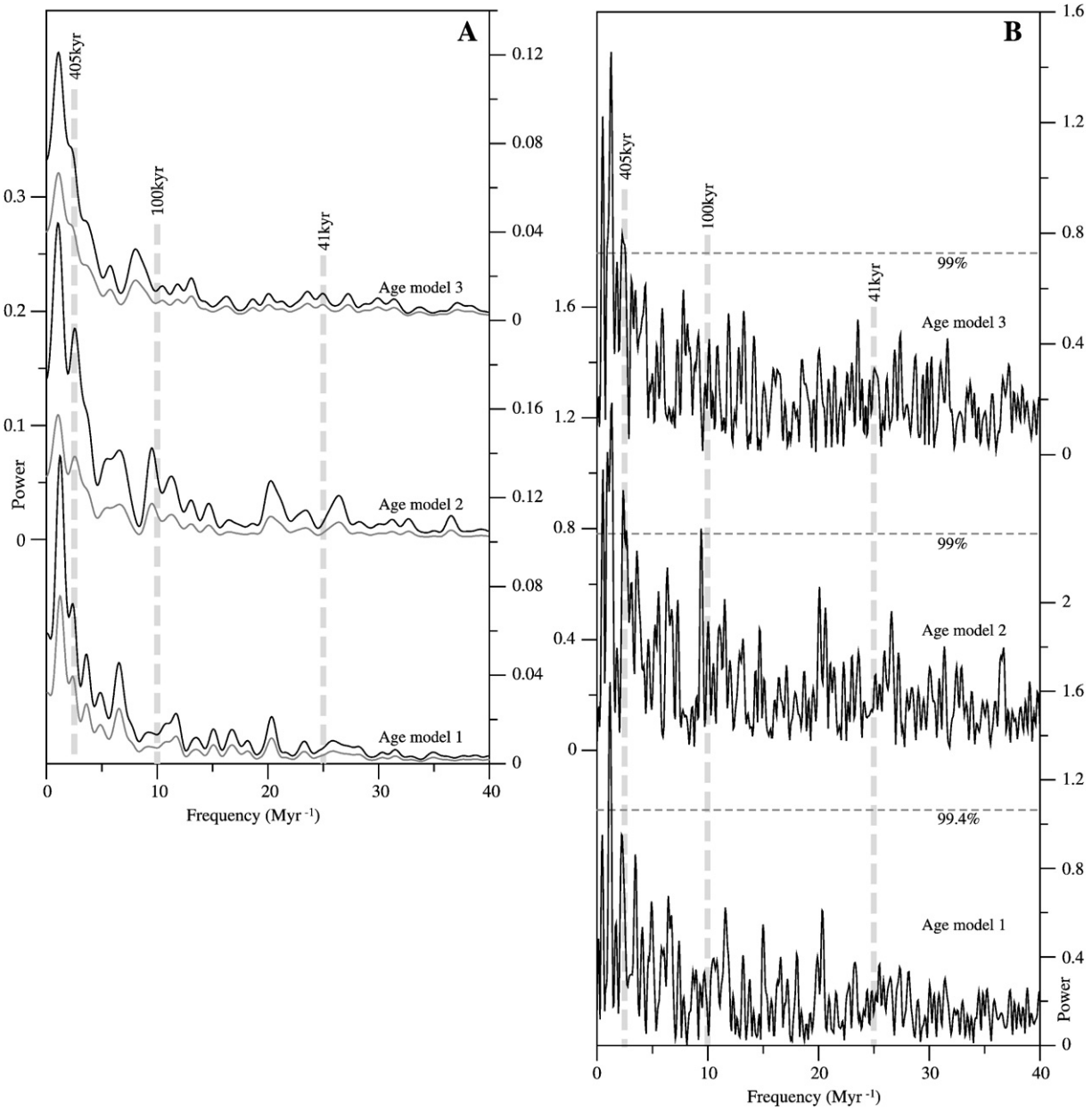

Fig. 6. The Blackman–Tuckey (A) and CLEAN red noise (B) power spectra of the L* time series according to the three age models (see text for explanation). In light grey, the 90% confidence limit is shown for the BT analysis (A). The horizontal dotted line indicates the 99% confidence interval of the CLEAN spectrum (B). Vertical lines indicate frequencies of obliquity, short and long eccentricity.

respectively (Fig. 5). In case a relation would exist, lithology thus also has a lagged, opposite phase relation to 2.4-Myr eccentricity. Nodes in obliquity amplitude related to the 1.2-Myr cycle were suggested to have a large impact on terrestrial climate (van Dam et al., 2006). In the obliquity time series, such nodes occur at around 13.8, 12.6, and 11.4 Ma. These do not show a relation with lithology and L* colour record in the VDA–MX section (Fig. 5).

5. Discussion

5.1. Million-year scale astronomical forcing

The transition from siliciclastic to carbonate-rich intervals at 2.4-Myr eccentricity minimum is identical to the relation found for a similar lithologic transition of Late Miocene age in the Cascante

Fig. 5. In the left; stratigraphic position, labelling of sequences and limestone beds (see caption Fig. 2), interpreted magnetostratigraphy, and lithology of the VDA–MX composite section, the L* record and its 17-points moving average, the sedimentation rates per resolved chron (interval) according to the ATNTS04 time scale (Lourens et al., 2004). In the middle; the tie-points used for the time series, the interpreted polarity with codes, and suggested correlation to the ATNTS04 time scale. Age model 1 uses tie-points marked with −, Age model 2 uses tie-points of Age model 1 and tie-points marked with ±, while Age model 3 uses all marked tie-points. To the right the eccentricity and obliquity target curves of the La2004 (1,1) solution of Laskar et al. (2004) and their low frequency filters of respectively 2.4-Myr and 1.2-Myr. Both the carbonate-rich intervals of the lower and upper sequence, shown with light-grey shading from the lithological column correlated to the time domain, start just after a minimum in the 2.4-Myr eccentricity cycle. More to the right, the magnetostratigraphic dating of the genetic sequences in the north-eastern and central portions of the Madrid Basin from this study and by Montes et al. (2006), respectively. Grey shades indicate that these intervals have not been directly dated, but dating of boundaries has been done by extrapolation of sedimentation rates. Labelling of the stratigraphic intervals of Montes et al. (2006) is slightly different from the labelling used here.

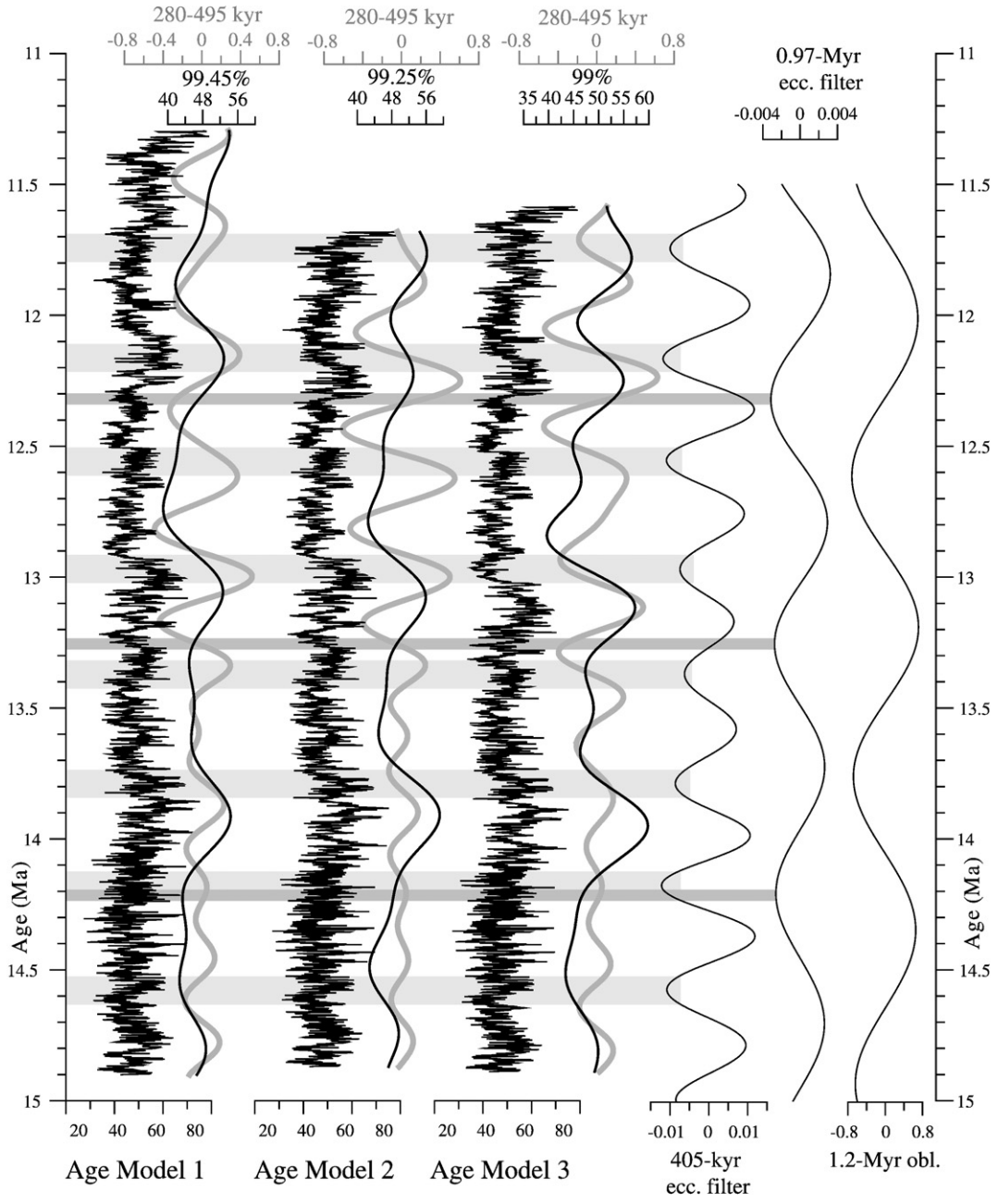

Fig. 7. The L* time series according to Age models 1, 2, and 3, their 280–495-kyr Bandpass filters in light grey, and the 99% and 99.4% reconstructed time series following the CLEAN method. To the right the 405-kyr and 0.97-Myr eccentricity, and 1.2-Myr obliquity cycles are shown, derived from filtering the eccentricity target curve and the amplitude modulator curves obliquity, respectively. Horizontal bars indicate minima in the 405-kyr and 0.97-Myr eccentricity cycles.

section in the Teruel Basin (Abels et al., 2009a). Van Dam et al. (2006) indicate that humidity adapted rodents migrated from central Europe to Spain during 2.4-Myr eccentricity minima, possibly indicating favourable conditions for lake expansion. In an attempt to explain the rather long phase lags, Abels et al. (2009a) suggested that the delayed response of the lithologic transition to 2.4-Myr eccentricity in the Teruel Basin might be related to a memory effect of groundwater reservoirs. This would mean that large groundwater reservoirs in the surroundings of the basin slowly fill and prevent water from directly flowing into the basin when net precipitation is enhanced and also when precipitation finally decreases these reservoirs keep delivering water to the basin for a certain time. Sanz et al. (1995) put forward that groundwater plays an important role in feeding the paleosol and pond environments in the Madrid Basin. Here, we propose that a prolonged period devoid of extreme evaporative conditions, due to low precession amplitudes and therefore lack of extremes at times of minimum eccentricity, might have filled groundwater reservoirs. After a certain time, a threshold value for carbonate deposition was crossed due to raised groundwater and/or lake levels, possibly assisted by positive feedback mechanisms like enhanced vegetation cover and increased chemical instead of physical weathering. However, it should be noted that before further explanations are made, it has to be corroborated whether the genetic sequences with a siliciclastic and a carbonate-rich interval in the Madrid Basin are indeed (partly) controlled by the 2.4-Myr eccentricity cycle. Also, the exact phase relation can only be measured when it is clear which mechanism, or part of the eccentricity cycle, forced the lithological transitions. Therefore, additional sequences in the Madrid Basin and other basins must be studied and also, rather important, the rough synchrony of the calcareous intervals in the segment of the Madrid

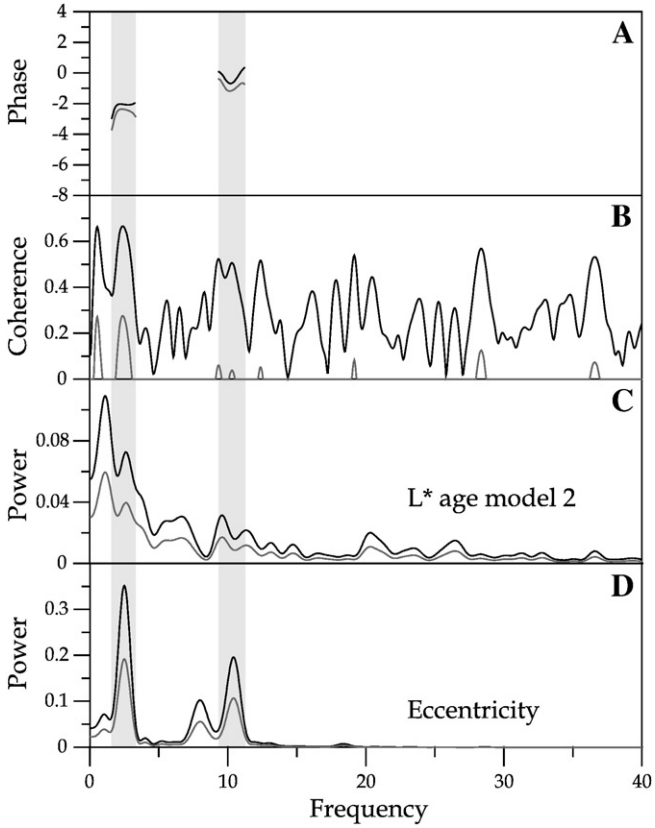

Fig. 8. Blackman–Tuckey cross-spectral analysis of the eccentricity and L* time series according Age model 2. The BT power spectrum of eccentricity (D) and L* time series (C), and the coherence (B) and phase diagrams (A) are shown. Light-grey lines indicate 90% confidence limit. Grey vertical bars indicate the short and long eccentricity frequency.

Basin that was hydrologically and physically connected with the VDA–MX area during deposition must be proven. For the moment, it is intriguing that exactly the same phase relation has been found for the single transition dated in the Teruel Basin (Abels et al., 2009a) and the two, possibly three, in the Madrid Basin.

The data reveal an opposite phase relation to eccentricity of the 405-kyr lithological cyclicity with respect to the 0.97-Myr and 2.4-Myr related cyclicity. Again, discussing these phase relations depends on the degree of certainty of the relation and the character of this relation between the orbital curve and the paleoenvironment. Nevertheless, we try to explain the phase relation between eccentricity and lithology as if eccentricity extremes, i.e. maxima and minima, forced the paleoenvironmental transitions, which would be most obvious. The 405-kyr cyclicity may have originated from subsequent relatively wet conditions related to high amplitude precession cycles during eccentricity maxima. In the mean time, the million-year scale eccentricity cyclicity may have originated from the prolonged absence of relatively dry and evaporative conditions. To verify such an hypothesis, the observed opposite phase relations should be further investigated by carrying out transient runs of global or regional scale climate models depicting eccentricity-scale climate forcing and local basin factors.

Van Dam et al. (2006) indicate that cooler and drier conditions prevailed on the Spanish mainland during long-period obliquity minima (nodes), probably due to increased global ice volume. They suggest that lacustrine limestone intervals are replaced by siliciclastic intervals (red beds) during these obliquity nodes. In the VDA–MX section, we have no indication for long-period obliquity forcing, and alternatively we suggest that the million-year scale termination of lacustrine phases is related to 0.97-Myr and 2.4-Myr eccentricity maxima.

5.2. Basin-wide correlations

An age of 15.6 Ma is obtained for the transition from the Lower to Intermediate Units by extrapolation of sedimentation rates in combination with adding 20 extra meters (Fig. 5; Alonso Zarza, 1990; Alonso Zarza et al., 1990). Montes et al. (2006) have dated magnetostratigraphically the Lower to Intermediate Unit boundary in the central and southern parts of the Madrid Basin and arrive at an age of 14.4 Ma. This age is in close agreement with nearby mammal sites. In the north-eastern parts of the basin, this boundary is now estimated at 15.6 Ma. The Lower to Intermediate Unit transition is thus not synchronous between the central and north-eastern portions of the basin (Fig. 5).

The transition from the lower to the upper sequence in the Intermediate Unit is dated here at 13.0 Ma, at the top of chron C5AAn. Montes et al. (2006) date this transition in the central parts of the basin at ca 13.4 Ma. An approximate 0.4 Myr age difference between the central and north-eastern parts of the basin is not very large, although the top of chron C5AAn, which marks the transition at VDA–MX, is correlated stratigraphically much higher in the Cerro de los Guardias section (Montes et al., 2006). In addition, in the central parts a third sequence within the Intermediate Unit is recognized, which seems not to be present in the north-eastern segment of the basin.

Above the MX section, an additional 20 m is measured until the top of the upper sequence and the Intermediate Unit is reached. Extrapolation of the sedimentation rate results in an age of ca 11 Ma for this boundary (Fig. 5). Two magnetostratigraphic correlation options result in rather different maximal ages of 11.8 Ma (option A) and 10.5 Ma (option B) for this same boundary in the central parts of the basin (Fig. 5).

In summary, the comparison of the bio-magnetostratigraphic dating of the Miocene infill in the north-eastern and central parts of the Madrid Basin indicates that the sequence boundaries as they are referred to in literature at present are not synchronous throughout the entire basin and their duration is different as well. This might indicate that the distinct areas evolved (partly) separately from each other. In the north-eastern segment, sedimentation varied drastically on a relatively small scale in response to major differences in geology of the basin margins (Calvo et al., 1989a; Alonso Zarza et al., 1992b). On a large scale, this impact might even have been larger. Also, the abundance of evaporites in the Lower Unit in the areas in the west of the basin may have led to an uneven landscape over which the Intermediate Unit was deposited (Megias et al., 1981; Calvo et al., 1989b). In such a way, topographic differentiation during sedimentation could have resulted in poor or no physical and/or hydrological contact between the areas. To further unravel the depositional history of the sequential units in the Miocene infill of the basin, additional (intermediate) sedimentary successions have to be studied and dated accurately.

5.3. High-frequency orbital forcing

No indication for ~100-kyr eccentricity, obliquity nor precession forcing has been found with the statistical analysis of the L* time series in the VDA–MX section. The lack of high-frequency orbital forcing in the VDA–MX section can have different causes. First, the magnetostratigraphy is not sufficiently accurate in all intervals of the section, and the polarity time scale probably not precise enough in the early middle Miocene as in this interval the scale is not astronomically calibrated (Lourens et al., 2004). Second, the succession might be discontinuous at smaller time scales, and different episodes of shallow lacustrine, pond, and (pedogenic) calcrete development can lead to vertical stacking of limestone beds, thereby masking high-frequency

cyclicity. Third, although the colour reflectance data in the VDA–MX reflects the carbonate content of the sediment in an appropriate way, it might not always be a perfect proxy for lithology and with that paleoenvironment. Carbonate precipitation occurred under different depositional conditions varying from calcic paleosols to pond and marginal lacustrine water bodies (Sanz et al., 1995). This means that variable local groundwater conditions may have resulted in similar colour patterns and thus in a similar imprint in the L* colour record. To further explore the high-frequency orbital cyclicity, a lithology rank should be made such that the colour reflectance data can be tested against paleoenvironment or the rank data series can be directly used for statistical analysis. Construction of a depth rank series will be a time-consuming effort, because carbonate petrography is needed at high resolution.

5.4. Middle Miocene climate variability

During the middle Miocene, a major global climate transition occurred presumably due to growth of the East Antarctic Ice Sheet (Miller et al., 1991; Flower and Kennet, 1994). In the Mediterranean, this transition has been accurately recorded and dated in a marine succession on Malta at 13.82 ± 0.03 Ma (Abels et al., 2005). A major small-mammal turnover occurred in the Spanish mainland from 14.3 Ma to 13.3 Ma with a peak at 13.75 Ma, thus roughly coincident with the climate shift (van der Meulen et al., 2005). The faunal change indicates a shift from drier to more humid conditions. At VDA–MX, the middle Miocene global cooling does not seem to have major impact as from 14.2 to 13.0 Ma continuous carbonate deposition occurred before and after the timing of the transition (Fig. 5). The start of small-mammal turnover however coincides with the base of the carbonate-rich interval of the lower sequence. To prove a common origin, additional climatic proxy data across the climate cooling interval are needed.

Holbourn et al. (2007) and Raffi et al. (2006) provide high-resolution astronomically calibrated benthic oxygen and carbon isotope records from the Pacific and Atlantic over the time interval preceding the climate transition. Both records show a dominance of obliquity variability from 14.5 Ma to the middle Miocene climate transition at 13.85 Ma. Before and after this interval, ~100-kyr eccentricity related cycles prevailed (see also Holbourn et al., 2004). In the VDA–MX section, the globally obliquity-dominated interval corresponds to the upper half of the siliciclastic interval of the lower sequence (stratigraphic meter 30 to 60 in Figs. 2 and 5). This interval is characterised by regular lithologic cycles of around 4 to 4.5 m thick (Figs. 3C and 2) corresponding to ca 63 to 72 kyr according the magnetostratigraphic age model. This duration is in between the periods of obliquity and ~100-kyr eccentricity, indicating that the floodplain succession was not controlled by either of the two or was controlled by a combination of these orbital cycles. Global climate variations did probably not dominate Spanish mainland during this time interval, which is remarkable in the middle Miocene as major global climate change took place. Alternatively, (orbital) climate variations were not the dominant forcing mechanism in the VDA–MX paleoenvironment. This idea is strengthened by the presence of higher-frequency lithological alternations in the interval before 14.5 Ma in the VDA–MX section than after 14.5 Ma (Fig. 5), whereas the interval before 14.5 Ma is dominated by major 100-kyr ice-volume variability in Pacific and Atlantic records instead of 41-kyr obliquity after 14.5 Ma (Raffi et al., 2006; Holbourn et al., 2007).

6. Conclusions

A detailed magnetostratigraphic age model has been established for the VDA–MX composite section in the north-eastern segment of the Madrid Basin, which matches biostratigraphic age constraints. Direct comparison of the lithological log with orbital target curves indicates that the onset of the calcareous intervals in the sedimentary sequences occurred during 2.4-Myr eccentricity minima. This configuration is identical to that found for a similar lithofacies transition of Late Miocene age in the Teruel Basin and is suggested to be related to prolonged periods of weak evaporative conditions at times of 2.4-Myr eccentricity minima. Spectral analysis of the L* time series reveals imprints of the 405-kyr and 0.97-Myr eccentricity cycles. Response to the 2.4-Myr and 0.97-Myr eccentricity cycles occurred with an opposite phase relation than the response to the 405-kyr cycle, while all three eccentricity cycles show a consistent phase lag of a quarter of a cycle. The phase lags are suggested to relate to slow response of large groundwater reservoirs to climate change. No imprint of 41-kyr and 1.2-Myr obliquity cycles has been found, indicating dominance of local (orbital forcing) processes on the floodplain environment in the Madrid Basin at that time. The magnetostratigraphic age model further indicates that the sedimentary sequences, since long recognized and correlated in the Miocene infill of the basin, do not represent time-equivalent sediment packages, and that their boundaries are diachronous. This suggests that these sequences are not of common origin within the whole basin, but rather that the different segments of the basin (partly) evolved separately.

To corroborate the suggestion of long-period orbital forcing on sequence formation in the Madrid Basin, the synchrony of sequences has to be proven for that part of the basin that was hydrologically and physically in contact during deposition. Subsequently, other sequences in the Madrid Basin as well as in other Cenozoic basins on the Iberian Peninsula have to be dated in the same way to test whether a similar orbital configuration existed during the deposition of calcareous intervals of the large-scale sequences, or if we are misled by three coincidences.

Acknowledgements

Bet Beamud, Mark Dekkers, Miguel Garcés, and Tom Mullender are thanked for paleomagnetic sampling, measuring, and interpretation assistance. We thank Manolo Montes, Jan van Dam, and Karel Steensma for discussion in the field. H.A. acknowledges the Dutch Science Foundation (NWO-ALW) for financial support. We acknowledge the thorough reviews of two anonymous colleagues.

References

Abdul Aziz, H., Krijgsman, W., Hilgen, F.J., Wilson, D.S., Calvo, J.P., 2003. An astronomical polarity timescale for the late middle Miocene based on cyclic continental sequences. J. Geophysical Research 108. doi:10.1029/2002JB001818.

Abdul Aziz, H., Van Dam, J.A., Hilgen, F.J., Krijgsman, W., 2004. Astronomical forcing in upper Miocene continental sequences: implications for the Geomagnetic Polarity Time Scale. Earth Planet. Sci. Lett. 222. doi:10.1016/j.epsl.2004.02.018.

Abels, H.A., Hilgen, F.J., Krijgsman, W., Kruk, R.W., Raffi, I., Turco, E., Zachariasse, W.J., 2005. Long-period orbital control on middle Miocene global cooling: integrated stratigraphy and astronomical tuning of the Blue Clay Formation on Malta. Paleoceanography 20. doi:10.1029/2004PA001129.

Abels, H.A., Abdul Aziz, H., Calvo, J.P., Tuenter, E., 2009a. Shallow lacustrine microfacies document orbitally paced lake-level history in the Miocene Teruel Basin (NE Spain). Sedimentology 56, 399–419.

Abels, H.A., Abdul Aziz, H., Ventra, D., Hilgen, F.J., 2009b. Orbital climate forcing in mudflat to marginal lacustrine deposits in the Miocene Teruel Basin (Northeast Spain). J. Sediment. Res. 79, 831–847.

Alonso Zarza, A.M., 1990. Estudio petrologico y sedimentologico de las facies de abanicos aluviales del Neogeno en el sector NE de la Cuenca de Madrid y su relacion con las facies mas centrales, Provincia de Guadalajara. Thesis doctoral, Universidad Complutense de Madrid, Madrid, Spain.

Alonso Zarza, A.M., Calvo, J.P., 2002. Tajo Basin. In: Gibbons, W., Moreno, T. (Eds.), The Geology of Spain. The Geological Society, London, pp. 315–320.

Alonso Zarza, A.M., Calvo, J.P., García del Cura, M.A., 1990. Litoestratigrafia y evolución paleogeografica del Mioceno del borde NE de la cuenca de Madrid (Prov. Guadalajara). Estud. Geol. 46, 415–432.

Alonso Zarza, A.M., Calvo, J.P., García del Cura, M.A., 1992a. Palustrine sedimentation and associated features – grainification and pseudo-microkarst – in the middle Miocene (Intermediate unit) of the Madrid Basin, Spain. Sediment. Geol. 76, 43–61.

Alonso Zarza, A.M., Wright, V.P., Calvo, J.P., García del Cura, M.A., 1992b. Soil-landscape and climatic relationships in the middle Miocene of the Madrid Basin. Sedimentology 39, 17–35.

Beaufort, L., 1994. Climatic importance of the modulation of the 100 kyr cycle inferred from 16 m.y. long Miocene records. Paleoceanography 9, 821–834.

Calvo, J.P., Alonso Zarza, A.M., García del Cura, M.A., 1989a. Models of Miocene marginal lacustrine sedimentation in response to varied depositional regimes and source areas in the Madrid Basin (central Spain). Palaeogeogr. Palaeoclimatol. Palaeoecol. 70, 199–214.

Calvo, J.P., Ordóñez, S., García del Cura, M.A., Hoyos, M., Alonso Zarza, A.M., Sanz, E., Rodriquez-Aranda, J.P., 1989b. Sedimentología de los complejos lacustres miocenos de la cuenca de Madrid. Acta Geol. Hisp. 24, 281–298.

Calvo, J.P., Alonso Zarza, A.M., García del Cura, M.A., Ordóñez, S., Rodriquez-Aranda, J.P., Sanz Montero, M.E., 1996. Sedimentary evolution of lake systems through the Miocene of the Madrid Basin: paleoclimatic and paleohydrological constraints. In: Friend, P.F., Dabrio, C.J. (Eds.), Tertiary Basins of Spain: the Stratigraphic Record of Crustal Kinematics. : World and Regional Geology, vol. 6. Cambridge University Press, Cambridge, pp. 272–277.

Cañaveras, J.C., Calvo, J.P., Hoyos, M., Ordóñez, S., 1996. Paleomorphologic features of an intra-Vallesian paleokarst, Tertiary Madrid Basin: significance of paleokarstic surfaces in continental basin analysis. In: Friend, P.F., Dabrio, C.J. (Eds.), Tertiary Basins of Spain: the Stratigraphic Record of Crustal Kinematics. World and Regional Geology, vol. 6. Cambridge University Press, Cambridge, pp. 279–284.

Daams, R., van der Meulen, A.J., Sierra, M.A.A., Peláez-Campomanes, P., Krijgsman, W., 1999. Aragonian stratigraphy reconsidered, and re-evaluation of the middle Miocene mammal biochronology in Europe. Earth Planet. Sci. Lett. 165, 287–294.

Flower, B.P., Kennet, J.P., 1994. The middle Miocene climatic transition: East Antarctic ice sheet development, deep ocean circulation and global carbon cycling. Palaeogeogr. Palaeoclimatol. Palaeoecol. 108, 537–555.

Heslop, D., Dekkers, M.J., 2002. Spectral analysis of unevenly spaced climatic time series using CLEAN: signal recovery and derivation of significance levels using a Monte Carlo simulation. Phys. Earth Planet. Inter. 130, 103–116.

Holbourn, A., Kuhnt, W., Schulz, M., 2004. Orbitally paced climate variability during the middle Miocene: high resolution benthic foraminiferal stable-isotope records from the tropical western Pacific. In: Clift, P, Kuhnt, W., Wan, P., Hayes, D. (Eds.), Continent–ocean Interactions within East-Asian Marginal Seas. Geophysical Monograph Series, vol. 149. American Geophysical Union, Washington DC, pp. 321–337.

Holbourn, A., Kuhnt, W., Schulz, M., Flores, J.A., Andersen, N., 2007. Orbitally-paced climate evolution during the middle Miocene "Monterey" carbon-isotope excursion. Earth Planet. Sci. Lett. 261, 534–550.

Kirschvink, J.L., 1980. The least-squares line and plane and the analysis of paleomagnetic data. Geophys. J. R. Astron. Soc. 62, 699–718.

Laskar, J., Robutel, P., Joutel, F., Gastineau, M., Correia, A.C.M., Levrard, B., 2004. A long term numerical solution for the insolation quantities of the Earth. Astron. Astrophys. 428, 261–285.

Lourens, L.J., Hilgen, F.J., 1997. Long-periodic variations in the earth's obliquity and their relation to third-order eustatic cycles and late Neogene glaciations. Quat. Int. 40, 43–52.

Lourens, L.J., Hilgen, F.J., Shackleton, N.J., Laskar, J., Wilson, D.S., 2004. The Neogene Period. In: Gradstein, F.M., Ogg, J.G., Smith, A. (Eds.), A Geolologic Time Scale 2004. Cambridge University Press, Cambridge, pp. 405–440.

Megias, A.G., Ordóñez, S., Calvo, J.P., 1981. Tertiary clastic gypsum deposits in the Madrid Basin. Regional Meeting Internation Association of Sedimentologists, pp. 109–112.

Miller, K.G., Wright, J.D., Fairbanks, R.G., 1991. Unlocking the ice house: Oligocene–Miocene oxygen isotopes, eustasy, and margin erosion. J. Geophys. Res. 96, 6829–6848.

Montes, M., Beamud, B., Garcés, M., Calvo, J.P., 2006. Magnetoestratigrafía de las unidades inferior e intermedia del miocene de la cuenca de Madrid. Rev. Soc. Geol. Esp. 19, 281–298.

Olsen, P.E., 1986. A 40-million-year lake record of early Mesozoic orbital climate forcing. Science 234, 842–848.

Olsen, P.E., Kent, D.V., 1999. Long-period Milankovitch cycles from the Late Triassic and Early Jurassic of eastern North America and their implications for the calibration of the early Mesozoic time-scale and the long-term behaviour of the planets. Philos. Trans. Math. Phys. Eng. Sci. 357, 1761–1786.

Paillard, D.L., Labeyrie, L., Yiou, P., 1996. Macintosh program performs time-series analysis. EOS Trans. AGU 77, 379.

Pälike, H., Frazier, J., Zachos, J.C., 2006. Extended orbitally forced palaeoclimatic records from the equatorial Atlantic Ceara Rise. Quat. Sci. Rev. 25, 3138–3149.

Pelaez-Campomanes, P., Azanza, B., Calvo, J.P., Daams, R., Herráez, E., Morales, J., Nieto, M., Soria, D., 2000. Bioestratigrafía de las faunas de mamíferos del Mioceno de Madrid: datación de las unidades estratigráficas. In: Morales, J. (Ed.), Patrimonio paleontológico de la Comunidad de Madrid. Serie de la Consejería de Educación, Comunidad de Madrid, Madrid, pp. 103–129.

Raffi, I., Backman, J., Fornaciari, E., Pälike, H., Rio, D., Lourens, L.J., Hilgen, F.J., 2006. A review of calcareous nannofossil astrobiochronology encompassing the past 25 million years. Quat. Sci. Rev. 25, 3113–3137.

Sanz, M.E., Alonso Zarza, A.M., Calvo, J.P., 1995. Carbonate pond deposits related to semi-arid alluvial systems: examples from the Tertiary Madrid Basin, Spain. Sedimentology 42, 437–452.

Sesé, 2006. Los roedores y lagomorfos del Neógeno de España. Estud. Geol. 62 (1), 429–480.

Sesé, C., Alonso Zarza, A.M., Calvo, J.P., 1990. Nuevas faunas de micromammiferos del terciario continental del NE de la cuenca de Madrid (Prov. de Guadalajara, España). Estud. Geol. 46, 433–451.

Shackleton, N.J., Crowhurst, S.J., Weedon, G.P., Laskar, J., 1999. Astronomical calibration of Oligocene–Miocene time. Philos. Trans. R. Soc. Lond. A 357, 1907–1929.

van Dam, J.A., Abdul Aziz, H., de los Angeles Alvarez Sierra, M., Hilgen, F.J., van den Hoek Ostende, L.W., Lourens, L.J., Mein, P., van der Meulen, A.J., Pelaez-Campomanes, P., 2006. Long-period astronomical forcing of mammal turnover. Nature 443, 687–691.

van der Meulen, A.J., Pelaez-Campomanes, P., Levin, S.A., 2005. Age structure, residents, and transients of Miocene rodent communities. Am. Nat. 165, E108–E125.

Varadi, F., Runnegar, B., Ghil, M., 2003. Successive refinements in long-term integrations of planetary orbits. Astrophys. J. 592, 620–630.

Wade, B.S., Pälike, H., 2004. Oligocene climate dynamics. Paleoceanography 19. doi:10.1029/2004PA001042.

Zijderveld, J.D.A., 1967. A.C. demagnetization of rocks: analysis of results. In: Collison, D.W., Creer, K.M., Runcorn, S.K. (Eds.), Developments in Solid earth Geoscience Methods in Palaeomagnetism. Elsevier Publishing Company, Amsterdam.